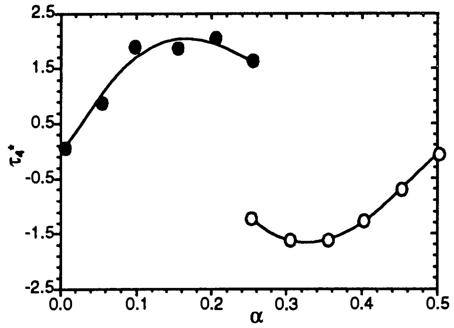

Fig. 4. Shear stress (τ_4^*) as a function of registry for stable phases under the conditions given in Fig. 2.

If the upper wall were permitted to float (under zero applied shear stress, $\tau_4 = 0$) on the film, it would come to rest with a registry corresponding to the minimum of ϕ. Under the conditions of our simulations, ϕ is minimum at either $\alpha = 0.0$ or 0.5, where, respectively, odd- and even-layer solid films exist. For instance, at $\tau_3^* = -0.598$ and -1.196, the one-layer solid at $\alpha = 0.0$ is stable; at $\tau_3^* = 0.0$, the walls adjust so that $\alpha = 0.5$ and the two-layer phase forms.

The shear stress τ_4^* oscillates between positive and negative values as the film is sheared (α increases) (Fig. 4). When the walls are in registry ($\alpha = 0.0$), the stable phase is a one-layer phase, which resists shearing by exerting a force on the walls opposing the (positive) applied shear stress, that is, in the direction of decreasing α. However, when α exceeds a critical value, the imbibition transition yields the more stable two-layer phase. As α increases beyond the critical value, the GI potential of the two-layer phase decreases. The strained phase now exerts a force on the walls in the direction of increasing α, which gives rise to a negative applied shear stress. The periodic sharp drops in frictional force below the baseline observed in the "super-kinetic" sliding state of the SFA (*14*) may reflect alternating imbibition and drainage transitions analogous to the ones described here.

REFERENCES AND NOTES

1. P. F. Low, *Langmuir* 3, 181 (1987).
2. F. M. Etzler and W. Drost-Hansen, in no. 188 of the *Advances in Chemistry Series*, M. Blank, Ed. (American Chemical Society, Washington, DC, 1980), p. 486.
3. S. Granick, *Science* 253, 1374 (1991).
4. J. N. Israelachvili, P. M. McGuiggan, A. M. Homola, *ibid.* 240, 189 (1988).
5. J. van Alsten and S. Granick, *Phys. Rev. Lett.* 61, 2570 (1988).
6. M. L. Gee, P. M. McGuiggan, J. N. Israelachvili, *J. Chem. Phys.* 93, 1895 (1990).
7. M. Schoen, C. L. Rhykerd Jr., D. J. Diestler, J. H. Cushman, *Science* 245, 1223 (1989).
8. P. A. Thompson and M. O. Robbins, *ibid.* 250, 792 (1990); M. O. Robbins and P. A. Thompson, *ibid.* 253, 916 (1991).
9. M. Lupkowski and F. van Swol, *J. Chem. Phys.* 95, 1995 (1991).
10. M. Schoen, D. J. Diestler, J. H. Cushman, *Phys. Rev. B* 47, 5603 (1993).
11. D. J. Diestler, M. Schoen, J. H. Cushman, in preparation.
12. S. G. Ash, D. H. Everett, C. Radke, *Faraday Trans. 2* 69, 1256 (1973).
13. M. Schoen, D. J. Diestler, J. H. Cushman, *J. Chem. Phys.* 87, 5464 (1987).
14. H. Yoshizawa, P. McGuiggan, J. Israelachvili, *Science* 259, 1305 (1993).
15. This work was supported by the U.S. Department of Energy, Office of Health and Environmental Research (DE-FG02-86ER-60310), and the U.S. Army Research Office (DAAL03-90-G-0074). The authors are grateful for time on the CRAY Y-MP/832 of the Höchsleistungsrechzentrum at the Forschungszentrum Jülich.

18 May 1993; accepted 8 September 1993

Long-Range Attractive Force Between Hydrophobic Surfaces Observed by Atomic Force Microscopy

Yi-Hua Tsao, D. Fennell Evans, H. Wennerström

There is evidence from atomic force microscopy for a long-range attractive force between hydrophobic surfaces that is virtually identical to that observed with the surface forces apparatus. This force is present in the nonaqueous solvent ethylene glycol. A possible molecular mechanism involves in-plane polarized domains of solid-like monolayers adsorbed on mica, and a theoretical model has been developed that accounts for many of the observations.

Hydrophobic interactions guide molecular self-assembly processes in biology and in many technological processes. It is known that hydrophobic interactions are proportional to the contact area both on the molecular and the colloidal (macroscopic) scale. However, little is known about the range of the hydrophobic forces, which is an important point in understanding the dynamics of self-organizing processes such as protein folding, ligand binding to hydrophobic receptor sites, and the transformation of membrane structures.

Reports published over the past decade (*1–5*) document the existence of long-range, strongly attractive forces between macroscopic hydrophobic surfaces immersed in water. These forces are orders of magnitude larger than that expected from van der Waals interactions and exhibit decay lengths of up to 25 nm. The molecular origin of these unusual forces is not well understood. None of the proposed mechanisms—which include water structural effects (*2*), Debye screened ion-ion or dipole-dipole correlations (*6, 7*), or vapor cavitation (*3*)—account for the experimental observations. At issue is the question of whether these long-range attractive forces arise from hydrophobic interactions and whether they provide an additional attractive force that promotes biomolecular processes.

To date, all accurate measurements of this force have been made with the surface forces apparatus (SFA), for which hydrophobic surfaces are prepared by the deposition of a monolayer of a double-chained cationic surfactant onto a negatively charged mica surface. Here, we (i) give a brief review of previous SFA measurements; (ii) present results of atomic force microscopy (AFM) showing the existence of the long-range force for equivalent systems; (iii) establish the existence of a long-range attractive force in a nonaqueous solvent, ethylene glycol; (iv) investigate other hydrophobic surfaces, such as Teflon and polyethylene; and (v) propose a model that explains the molecular origin of the long-range attractive force.

Both the magnitude and the range of the long-range attractive force between two hydrophobic surfaces in water depend on the temperature and length of the surfactant's hydrocarbon chain. The SFA results (*5*) at 25°C (Fig. 1A) show that dioctadecyldimethylammonium (DODA), dieicosyldimethylammonium (DEDA), and didoeicosyldimethylammonium (DDDA) monolayers gave identical results, whereas the dihexadecyldimethylammonium (DHDA) monolayer yielded a substantially weaker attractive force. At 50°C (Fig. 1B), the force curve for DEDA remained identical to that measured at 25°C. Those for DHDA and DODA decreased substantially, and DHDA gave values comparable with those predicted by van der Waals theory (solid line). The force curves (Fig. 1) were integrated from double exponential functions that fit the SFA results. For example, the force curve for DODA at 25°C is

$$F/R = -\ 0.331\ e^{-D/2.1} - 0.00125\ e^{-D/25} \tag{1}$$

where F is the force in newtons, R is the radius of curvature of the surfaces in meters,

---

Y.-H. Tsao and D. F. Evans, Department of Chemical Engineering and Materials Science, University of Minnesota, Minneapolis, MN 55455.
H. Wennerström, Division of Physical Chemistry, The Chemical Center, University of Lund, S-22100 Lund, Sweden.

and D is the tip-surface spacing in nanometers. As shown in Table 1 (*8, 9*), changes in the force curves correlate with the chain melting temperatures of the surfactants. These observations suggest that the long-range attractive force is observed only when the chains are in a frozen, ordered state.

The AFM images (*5*) of the diakyl cationic monolayers in air and under water permit individual terminal methyl groups to be visualized and show that the monolayers were uniform, stable, and continuous over areas extending for several micrometers. The AFM images establish that when immersed in water, DODA and DEDA monolayers changed only slightly and show the long-range ordering expected for a crystalline array of frozen hydrocarbon chains. The images of the shorter chained DHDA reveal that their chain packing was less ordered than that for the two longer chain compounds.

Upon addition of salt ($\sim 10^{-4}$ M), the long-range attraction diminished rapidly, with multivalent ions such as magnesium showing a more pronounced effect than monovalent ions (*10*). Streaming potential measurements by Scales, Grieser, and Healy (*11*) show that the zeta-potential of the hydrophobic monolayer is -8 ± 5 mV in water and in 10^{-3} M KCl (*12*), establishing that the surfaces have a very small net charge.

Force measurements on asymmetric systems with one uncharged monolayer surface and one charged, bare mica surface yielded the surprising result that the force was slightly stronger and had a longer range than those observed between two symmetric monolayers (*10*). The dependence of the force on added salt was the same in both systems. The similarity in behavior between these two different systems suggests a common molecular origin.

The SFA measurements on the asymmetric systems prompted us to investigate these phenomena with AFM. The interaction force was measured when a pyramidal AFM tip approached a planar surface (*13*). In an aqueous solution, Si_3N_4 tips become negatively charged and behave in a manner similar to bare mica, which is also negatively charged (*14*). The AFM force curve for a Si_3N_4 tip approaching a bare mica surface in water displayed typical Derjaguin-Landau-Verwey-Overbeek (DLVO) behavior with a long-range electrostatic repulsion that turned into a short-range van der Waals attraction. The AFM force measurements were carried out with a Digital Instruments AFM equipped with a quartz liquid flow cell (*5*). The deflection of the cantilever spring was measured as the mica surface was moved toward the rigidly mounted cantilever-tip assembly. When the derivative of the force dF/dD exceeded the spring constant, the tip jumped into contact with the mica substrate. The spring constant of the cantilever was measured by the procedure suggested by Burnham and co-workers (*15*). We prepared hydrophobic monolayers by dipping mica or the Si_3N_4 AFM tips into warm cyclohexane solutions containing $\sim 2 \times 10^{-4}$ M surfactant for 5 min. The surfactant-coated surfaces were rinsed in warm cyclohexane to remove any excess surfactant and were dried (*5*). In addition, AFM images of the hydrophobic monolayer adsorbed on Si_3N_4 (*16*) (Fig. 2) are identical to those observed with the mica substrate.

Using the AFM, we measured the force between (i) a Si_3N_4 tip and a hydrophobic monolayer on mica; (ii) bare mica and a Si_3N_4 tip with a hydrophobic monolayer; and (iii) hydrophobic monolayers, on both mica and the tip (Fig. 3). Monolayers formed on Si_3N_4 were stable and continuous over several micrometers as observed by AFM. At separations of ≈ 5.0 nm from final contact, the force exceeded the spring constant of the AFM cantilever, and the tip jumped into contact with the mica sheet. Before the jump, there was, in all three cases, a long-range attraction much stronger than the expected van der Waals force, similar to the observations made with the SFA technique. As in the SFA experiments, in water and at room temperature, the force was weaker for the shorter chain DHDA monolayer than for the DODA, DEDA, and DDDA monolayers, which all gave forces of a similar magnitude. The force was stronger for the hydrophobic mica–bare tip case than for the bare mica–hydrophobic tip case, whereas for the symmetric situation of hydrophobic mica and tip, the force was substantially weaker. This agrees qualitatively with the observations made in the SFA experiments.

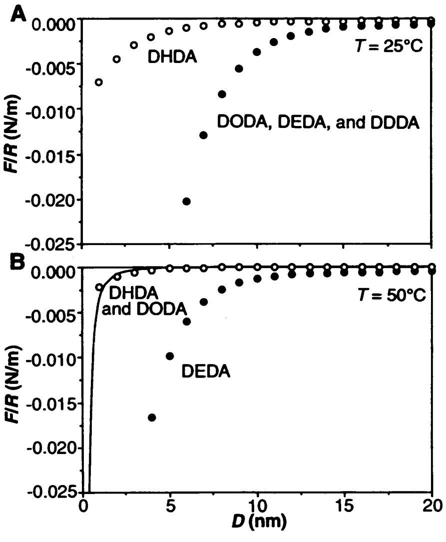

Fig. 1. Force curves from SFA measurements at (**A**) 25°C and (**B**) 50°C, obtained by integration of the double-exponential fit to the measured $d(F/R)/dD$ versus D. Circles represent measurements between DHDA, DODA, DEDA, or DDDA monolayers in water. Monolayer contact is set to be $D = 0$ in all cases. The solid line in (B) is the calculated nonretarded van der Waals force $F/R = -A/6D^2$, where the Hamaker constant $A = 1.8 \times 10^{-20}$ J. Comparison between the force curves for DEDA at 25° and 50°C establishes that the attractive forces are similar, whereas those for DHDA and DODA decrease and approach the van der Waals theoretical limit. Part of the data in (A) and all of the data in (B) are from (*5*).

To achieve a quantitative comparison, we must relate the force measured between a tip and a flat surface in an AFM experiment to that measured between two cylindrical surfaces in the SFA experiment. Pictures from a scanning electron microscope show that the tip has a general pyramidal shape with a rounded portion at the very end. Neglecting this latter feature, we model the tip as a four-sided pyramid with an

Table 1. Chain transition temperatures of dialkyldimethylammonium surfactants (*8, 9*).

Compound	In water (°C)	In ethylene glycol (°C)
DHDA-OAc	34	7
DODA-OAc	44	35
DEDA-Br	62	49
DDDA-Br	70	56

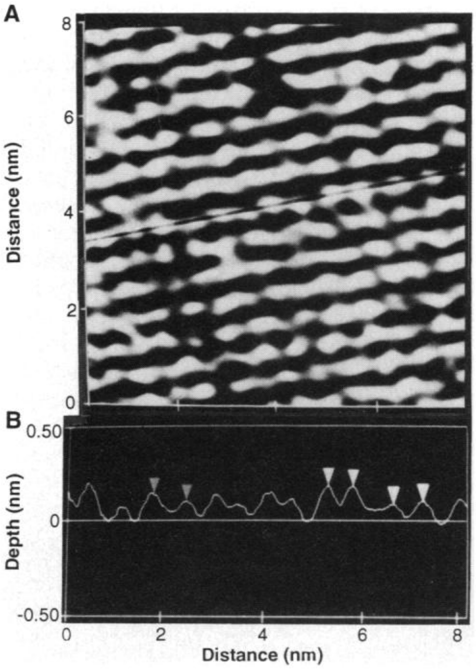

Fig. 2. (**A**) An AFM image of a DODA monolayer adsorbed on Si_3N_4 in air at 25°C. Individual methyl groups of the hydrocarbon chains can be identified. (**B**) Cross-sectional profile along the line drawn in the image. The two terminal groups associated with a DODA molecule (as indicated by the arrows) are separated by 0.5 to 6 nm.

apex angle α. Invoking the Derjaguin approximation (*17*), that the total force $F(D)$ is obtained by integration of the force $f(x)$ between surface patches of the tip and the planar surface, we find

$$F(D) = 8\tan^2\left(\frac{\alpha}{2}\right)\int_D^\infty f(x)(x-D)dx \quad (2)$$

If we assume that the long-range attractive force $f(x)$ measured in the SFA experiments has the same properties as that measured in the AFM experiments, then we can integrate Eq. 2 using $f(x) = d[F(x)/2\pi R]/dx$ from Eq. 1 to give

$$F(D) = -\tan^2\left(\frac{\alpha}{2}\right)(0.87\,e^{-D/2.1} + 0.04\,e^{-D/25}) \quad (3)$$

for the symmetrical DODA monolayers, where F is in nanonewtons and D is in nanometers. Estimated values of the apex angle lie in the range 70° to 100°. When $\alpha = 90°$ (solid line in Fig. 3A), there is excellent quantitative agreement between the two methods. We conclude that within the experimental uncertainty in α, we reproduced the SFA measurements quantitatively with the AFM technique.

An advantage of the AFM method is that it can readily be applied to a variety of surfaces and solvents. A long-range attractive force similar to that observed in water was also detected in ethylene glycol (Fig. 3B). In this solvent, the force was the same for the DDDA and DEDA surfactant monolayers but smaller for DODA. This quantitative difference reflects the lower melting temperature of the surfactants in ethylene glycol (Table 1) as compared with water. Parker and Claesson (*18*) observed a strong attractive force in mixed water–ethylene glycol systems, but our observation is of the long-range attractive force in a pure nonaqueous solvent.

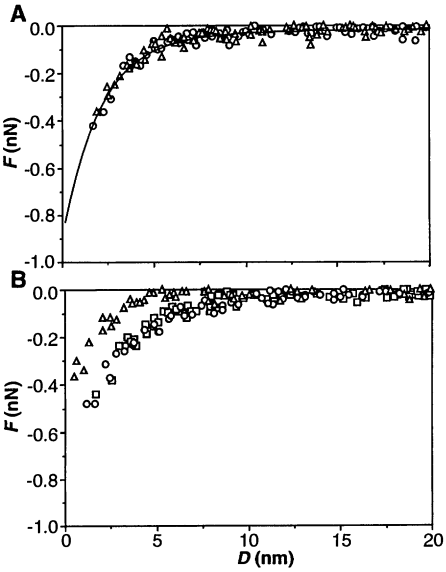

Fig. 3. (**A**) AFM force measurements between DODA monolayers, both on mica and on the Si_3N_4 tip, in water at 25°C. The circles and triangles represent two sets of measurements. The solid line is calculated from Eq. 3 with $\alpha = 90°$. (**B**) AFM force measurements between DODA (triangles), DEDA (squares), and DDDA (circles) monolayers, adsorbed on mica and a Si_3N_4 tip, in ethylene glycol at 25°C. Each set of data consists of two independent measurements.

No long-range attractive force was detected when a bare tip approached either Teflon or polyethylene surfaces in either water or ethylene glycol. We suggest that the specific molecular structures associated with solid hydrophobic monolayers adsorbed onto mica that give rise to the long-range attractive force are not present on these polymeric surfaces.

Key experimental observations were that the long-range attractive forces (i) were observed in both water and ethylene glycol and cannot be attributed to unique structural properties of water; (ii) occurred only when the hydrocarbon chains of the monolayer were in a solid state and disappeared upon heating, showing that the force depends on the detailed molecular properties of the surface; (iii) displayed similar magnitudes in both symmetric (two solvophobic monolayers) and asymmetric (a solvophobic monolayer and a bare, charged mica surface) systems, which rules out explanations based solely on solvophobic interactions; and (iv) showed an extreme sensitivity to the concentration and valency of added salt in both the symmetric and asymmetric systems, suggesting that Debye electrostatic shielding of charge-charge interactions must play a prominent role in both systems.

Consider the molecular structure of the monolayers. The area per negative charge on the mica surface is 49 to 50 Å^2. The smallest cross-sectional area of a hydrocarbon chain in its all-*trans* (solid) configuration is ≈19 or 38 Å^2 per surfactant molecule. With solid chains, this mismatch in cross-sectional areas leads to chains with tilted configuration and to the generation of monolayer structures possessing long-range order. Such tilted structures generate in-plane dipole moments. In the absence of screening, electrical fields would penetrate out into the solution on a length scale corresponding to the in-plane correlation length. Associated with increasing domain size is an increasing overall electrostatic energy. This situation is analogous to that observed with phospholipid monolayers at the air-water interface when two phases coexist, one forming domains in the other (*19*).

Two surfaces at large separations communicate when one becomes polarized in the electric field generated by the other. An attraction between the surfaces occurs when the polarization of the surface becomes larger than that of the medium. The range of the polarizing electrical field is determined by both the domain size and the screening from the electrolyte in the medium.

We model this attraction mechanism by considering the monolayer mica surface to be built up of circular (or hexagonal) domains of characteristic size R_D. These domains are assumed to have a surface charge density σ of a dipolar character

$$\sigma(r,\theta) = \sigma(r)\cos\theta \quad (4)$$

The maximum attraction results when domains on two opposing surfaces have dipolar orientations differing by 180°. We can estimate the effect of screening electrolyte by solving the Poisson-Boltzmann (PB) equation. By imposing a symmetry condition that electrical field lines remain within the cylinder between the two opposing circular domains and assuming that the potential is small, we can linearize the PB equation and obtain tractable solutions. For this case, the attractive force becomes

$$\frac{\text{force}}{\text{area}} = -\frac{1}{2\epsilon_o\epsilon_r}\sum_n a_n^2 \cosh^{-2}\left[\left(\kappa^2 + \frac{\gamma_{1n}^2}{R_D^2}\right)^{1/2}\frac{D}{2}\right] \quad (5)$$

where

$$a_n = \frac{\int_0^1 J_1(\gamma_{1n}x)\sigma(xR_D)xdx}{J_1(\gamma_{1n})(1-\gamma_{1n}^{-2})} \quad (6)$$

where $\epsilon_o\epsilon_r$ is the dielectric permittivity of the medium, κ^{-1} is the Debye screening length, J_1 is the first-order Bessel function, and γ_{1n} the nth zero of its first derivative.

A similar derivation for the asymmetric case characterized by one surface having a surface charge density $\sigma(r, \theta)$ as above and the second with a uniform surface potential Φ_0 yields

$$\frac{\text{force}}{\text{area}} = -\frac{1}{2\epsilon_o\epsilon_r}\sum_n a_n^2 \cosh^{-2}\left[\left(\kappa^2 + \frac{\gamma_{1n}^2}{R_D^2}\right)^{1/2} D\right] + \frac{1}{2\epsilon_o\epsilon_r}\Phi_0\sum_n\left(\kappa^2 + \frac{\gamma_{0n}^2}{R_D^2}\right)b_n^2\cosh^{-2}\left[\left(\kappa^2 + \frac{\gamma_{0n}^2}{R_D^2}\right)^{1/2} D\right] \quad (7)$$

where

$$b_n = \int_0^1 J_0(\gamma_{0n}x)xdx \quad (8)$$

J_0 is the zero-order Bessel function, and γ_{0n} is the nth zero of its first derivative. In the asymmetric case, the force involves a sum of an attractive domain correlation and a repulsive double-layer forces.

Equations 5 and 7 provide a qualitative explanation of the following observations: (i) adding electrolyte (that is, increasing κ) weakens the force; (ii) if $\sigma(r, \theta)$ scales with the domain size, then the force is independent of R_D for $R_D >> D$, $R_D >> \kappa^{-1}$, or both; (iii) as the domain size decreases with increasing temperature, a transition occurs from a regime where the force is insensitive to changes in R_D to a regime where the force decreases sharply with decreasing R_D; (iv) the magnitude of the force is consistent with reasonable values of σ; that is, $\sigma_{max} \approx 0.01$ C/m^2 is more than enough to yield the observed long-range forces; (v) attractive forces in the symmetric and asymmetric systems arise from the same basic mechanism; and (vi) if, in the asymmetric case, the attractive component wins over the repulsive at some separation, it does so at all separations.

However, Eqs. 5 and 7 do not explain the data quantitatively. In particular, (i) contrary to observations, the force is predicted to be weaker in the symmetric case than in the asymmetric case and (ii) the predicted dependence on κ is too weak to quantitatively account for the observations. In our view, lack of agreement is partly caused by the approximation imposed by linearization of the PB equation. (iii) Finally, the above theory in combination with the van der Waals theory does not account for the strongly attractive component of the force that appears at the shorter range and has an apparent decay constant in the range 1.5 to 3.5 nm. This short-ranged interaction may directly measure the hydrophobic attraction; however, it could equally well arise by domain correlation combined with a rearrangement of domain sizes caused by the interaction between the surfaces as they move together.

REFERENCES AND NOTES

1. J. N. Israelachvili and R. M. Pashley, *Nature* **300**, 341 (1982).
2. R. M. Pashley, P. M. McGuiggan, B. W. Ninham, D. F. Evans, *Science* **229**, 1088 (1985).
3. H. K. Christenson, J. Fang, B. W. Ninham, J. L. Parker, *J. Phys. Chem.* **94**, 8004 (1990); and references therein.
4. K. Kurihara, S. Kato, T. Kunitake, *Chem. Lett.* **9**, 1553 (1990).
5. Y.-H. Tsao, S. X. Yang, D. F. Evans, H. Wennerström, *Langmuir* **7**, 3154 (1991).
6. F. Podgornik, *J. Chem. Phys.* **91**, 5840 (1989).
7. P. J. Attard, *J. Phys. Chem.* **93**, 6441 (1989).
8. Y. Okahata, R. Ando, T. Kunitake, *Bunsenges. Physik. Chem. Ber.* **85**, 789 (1981).
9. The chain melting temperatures of dialkyldimethylammonium surfactants in ethylene glycol were measured with a Perkin-Elmer DSC 7 differential scanning calorimeter.
10. Y.-H. Tsao, D. F. Evans, H. Wennerström, *Langmuir* **9**, 779 (1993).
11. P. J. Scales, F. Grieser, T. W. Healy, *Thin Solid Films* **215**, 223 (1992).
12. For further discussion, see (*10*).
13. G. Bennig, C. F. Quate, Ch. Gerber, *Phys. Rev. Lett.* **56**, 930 (1988).
14. L. Bergstrom and R. J. Pugh, *J. Am. Ceram. Soc.* **72**, 103 (1989); L. Bergstrom and E. Bostedi, *J. Colloid Interface Sci.* **49**, 183 (1990).
15. N. A. Burnham and R. J. Colton, in *Scanning Tunneling Microscopy: Theory and Applications*, D. Bonnel, Ed. (VCH, New York, 1992), chap. 2; G. Lee, thesis, University of Minnesota (1992).
16. One of the V-shaped cantilevers on a monolayer-coated AFM cantilever substrate (Digital Instruments) was removed and glued onto a stainless steel disk with the Si_3N_4-monolayer side up. An optical microscope was used to locate the monolayer-coated cantilever for the AFM imaging.
17. B. V. Derjaguin, *Kolloid Z.* **69**, 155 (1934).
18. J. L. Parker and P. M. Claesson, *Langmuir* **8**, 757 (1992).
19. H. M. McConnell, L. K. Tamm, R. M. Weis, *Proc. Natl. Acad. Sci. U.S.A.* **81**, 3249 (1984); H. Möhwald, *Annu. Rev. Phys. Chem.* **41**, 411 (1990).

20. This work was supported by the National Institutes of Health (GM34341).

19 April 1993; accepted 1 September 1993

A Direct Measurement of the Terrestrial Mass Accretion Rate of Cosmic Dust

S. G. Love and D. E. Brownlee

The mass of extraterrestrial material accreted by the Earth as submillimeter particles has not previously been measured with a single direct and precise technique that samples the particle sizes representing most of that mass. The flux of meteoroids in the mass range 10^{-9} to 10^{-4} grams has now been determined from an examination of hypervelocity impact craters on the space-facing end of the Long Duration Exposure Facility satellite. The meteoroid mass distribution peaks near 1.5 × 10^{-5} grams (200 micrometers in diameter), and the small particle mass accretion rate is (40 ± 20) × 10^6 kilograms per year, higher than previous estimates but in good agreement with total terrestrial mass accretion rates found by geochemical methods. This mass input is comparable with or greater than the average contribution from extraterrestrial bodies in the 1-centimeter to 10-kilometer size range.

The Earth's meteoritic mass accretion rate plays an important role in many contexts. It constrains models of the interplanetary meteoroid population and of the zodiacal light (*1*), facilitates assessment of the importance of exogenous materials both on other planets (*2, 3*) and in the development of life on Earth (*4–6*), provides calibration for the use of Os isotopes and Ir abundances as tracers for estimation of terrestrial sedimentation and large impact rates (*7–9*), imposes constraints on the influence of extraterrestrial ^{3}He in the isotopic composition of terrestrial materials (*10*), and quantifies meteoroid collision hazards for spacecraft. The Earth's accretion rate of meteoritic material in a single typical year is believed to be dominated by submillimeter particles (*4, 5, 9, 11*), as evidenced by spacecraft meteoroid detectors and optical and radar meteor studies, whereas the average contribution from 1000-ton and larger bodies may dominate the flux on longer time scales (*12–14*). Unfortunately, the implied peak of the micrometeoroid mass distribution occurs at particle sizes between 0.1 and 1.0 mm, where the flux is below the detection limit of previous spacecraft studies and the meteoroid kinetic energy is inadequate for mass determination by optical meteor techniques (*1, 11, 15*). Radar meteor studies sample this size range, but uncertainties in the extraction of meteoroid masses from radar echo data lead to a two orders of magnitude mismatch with the spacecraft-derived mass flux at the radar detection limit of ~10^{-6} g, leading to an at least half an order of magnitude uncertainty in the integrated micrometeoroid mass accretion rate derived by this method (*11*).

We have determined the mass flux and size distribution of micrometeoroids in the critical submillimeter size range by measuring hypervelocity impact craters found on the space-facing end of the gravity-gradient–stabilized Long Duration Exposure Facility (LDEF) satellite. A number of factors establish the unprecedented reliability of this approach: the large area and exposure time of the collection surfaces, their constant (always within 1°) zenith-pointing attitude, and a wealth of empirical data that allow projectile energies to be accurately determined from the sizes of craters in solid aluminum targets.

A set of 761 craters was found on 5.6 m^2 of "thermal control panel" surfaces exposed to space for 5.77 years at altitudes ranging from 480 to 331 km. The panels were

---

Department of Astronomy, FM-20, University of Washington, Seattle, WA 98195.